JMEPEG (2017) 26:5237–5250
DOI: 10.1007/s11665-017-3005-z

1059-9495/$19.00

Influences of Processing and Fatigue Cycling on Residual Stresses in a NiCrY-Coated Powder Metallurgy Disk Superalloy

T.P. Gabb, R.B. Rogers, J.A. Nesbitt, R.A. Miller, B.J. Puleo, D. Johnson, J. Telesman, S.L. Draper, and I.E. Locci

(Submitted September 15, 2017; published online October 16, 2017)

Oxidation and corrosion can attack superalloy disk surfaces exposed to increasing operating temperatures in some turbine engine environments. Any potential protective coatings must also be resistant to harmful fatigue cracking during service. The objective of this study was to investigate how residual stresses evolve in one such coating. Fatigue specimens of a powder metallurgy-processed disk superalloy were coated with a NiCrY coating, shot peened, and then subjected to fatigue in air at room and high temperatures. The effects of this processing and fatigue cycling on axial residual stresses and other aspects of the coating were assessed. While shot peening did induce beneficial compressive residual stresses in the coating and substrate, these stresses relaxed in the coating with subsequent heating. Several cast alloys having compositions near the coating were subjected to thermal expansion and tensile stress relaxation tests to help explain this response of residual stresses in the coating. For the coated fatigue specimens, this response contributed to earlier cracking of the coating than for the uncoated surface during long intervals of cycling at 760 °C. Yet, substantial compressive residual stresses still remained in the substrate adjacent to the coating, which were sufficient to suppress fatigue cracking there. The coating continued to protect the substrate from hot corrosion pitting, even after fatigue cracks initiated in the coating.

Keywords coatings, residual stress, superalloys

1. Introduction

Disk application temperatures of 700 °C and higher (Ref 1) can heighten oxidation and preferentially activate hot corrosion attack modes in harmful environments, to become important design life limitations. Even just oxidation from exposures at 700 °C and higher can impair the fatigue resistance of disk superalloys (Ref 2-4). This oxidation process includes the formation of oxide layers and changes in superalloy chemistry and phases adjacent to the oxide layers. While the formation of chromium oxide is known to be protective, other nickel, cobalt, and titanium oxides can also form that are considered not protective. Selective oxidation of certain elements can also result in the formation of a zone adjoining the oxide layers without the strengthening gamma prime precipitates, leaving only the weak gamma phase at these locations. This layer can sometimes also recrystallize resulting in a finer grain size than the original microstructure. The grain boundaries in this zone can be susceptible to cracking during fatigue at high temperatures, related in part to a lack of $Cr_{23}C_6$ carbides (Ref 4). These aspects of oxidation can lower fatigue life up to 98% due to cracking at the surface of disk superalloys.

T.P. Gabb, R.B. Rogers, J.A. Nesbitt, R.A. Miller, B.J. Puleo, D. Johnson, J. Telesman, and **S. L. Draper**, Materials and Structures Division, NASA Glenn Research Center, Cleveland, OH; and **I.E. Locci**, University of Toledo, Toledo, OH. Contact e-mail: tim.gabb@grc.nasa.gov.

Type II hot corrosion attack can occur at 700 °C to nearly 800 °C on superalloy surfaces (Ref 5-7) by the melting of ingested deposits containing mixtures of sodium, magnesium, and calcium sulfates, as well as by direct impingement of SO_2-containing exhaust gas. However, SO_2 gas is not necessary for hot corrosion attack. Salt deposits can liquefy as sulfates and react with surface oxides to make the oxide go into solution, becoming non-protective. This allows for hot corrosion attack of the newly exposed superalloy surface. The attack can be further enhanced at the grain boundaries in superalloys in certain conditions. Pits can form in some conditions, and general corrosion can occur in other conditions (Ref 7). The pits can act as geometric stress concentration sites, which accelerate crack initiation during mechanical fatigue loading. These aspects of both pits and uniform corrosion can also lower fatigue life up to 98% due to cracking at the surface of disk superalloys (Ref 3, 8-11).

For susceptible locations, a suitable metallic coating could provide protection of exposed disk surfaces from such oxidation and corrosion effects. For example, PtAl, NiAl, and NiCoCrAlY (Ref 12) coatings have been extensively developed to protect superalloy airfoils from oxidation and corrosion. However, these coatings have lower ductility and fatigue resistance than turbine disk superalloys, at turbine disk temperatures extending up to 760 °C. This is a serious concern, as an effective "protective" coating must not impair the fatigue resistance of the disk surfaces upon which it is applied, as disks are fatigue limited and fracture critical in aero-propulsion applications.

Many disk surfaces are shot peened after appropriate machining (Ref 13). Shot peening can produce a consistent surface finish and impart beneficial compressive residual stresses near the treated surfaces that impede fatigue cracking (Ref 14, 15). Protective coatings would need to be applied after fully machining a disk surface location, but could be introduced before shot peening, to take advantage of the potential benefits

of subsequent shot peening. For such an approach, the residual stresses and roughness generated by shot peening within the coating would need to be evaluated, in order to minimize the coating's effect on the disk's resistance to fatigue cracking, while still offering protection from oxidation and corrosion attack. The evolution of the coating's residual stresses and surface roughness with heating and fatigue cycling would need to be considered in this evaluation.

The objective of the study was to determine the axial residual stresses, fatigue resistance, and corrosion resistance of a powder metal nickel-based superalloy that had been coated with a NiCrY coating and then shot peened. The effects of associated specimen processing, heating, and fatigue cycling on residual stresses, roughness, fatigue cracking, and hot corrosion resistance were evaluated. Cast alloys having compositions near that of the coating were also tested, in order to help understand the coating's response.

2. Materials and Procedure

A nickel-chromium-yttrium coating was deposited on a PM disk superalloy LSHR for this study. The LSHR test material had the composition listed in Table 1. LSHR superalloy powder was atomized, consolidated, and extruded. Extrusion segments were isothermally forged into flat disks (Ref 16). Extracted blanks were supersolvus solution heat-treated at 1171 °C for 2 h in a resistance heating furnace, then consistently cooled in static air and subsequently age heat-treated at 855 °C for 4 h, followed by 775 °C for 8 h. The resulting LSHR grain microstructure is shown in Fig. 1(a), having an average linear intercept grain size of about 15 μm.

Samples of cast alloys 50-50Nb and UCX having compositions, Table 1, which were near that of the coating (''coating alloys''), were obtained courtesy of Kubota Metal Corporation. These materials were tested in the as-cast form, as used in many applications. Cast and wrought Nichrome, having a composition with lower Cr content than the other ''coating alloys,'' was purchased as a hot worked bar of 19 mm diameter. Their average linear intercept grain sizes ranged from 50 μm for Nichrome to 740 μm for UCX.

Fatigue specimens having uniform gage sections 6.4 mm in diameter were then machined of LSHR. Tensile specimens having uniform gage sections 4.1 mm in diameter and 19 mm long were machined out of LSHR and the coating alloys. Additional cylinders 6.4 mm in diameter were machined from all these materials to measure thermal expansion.

High-power impulse magnetron sputtering (HiPIMS) was employed by Southwest Research Institute to apply a Ni-45Cr-0.15Y (weight percent, nominal) coating. Prior to coating, the test specimen surface was prepared by grit blast using alumina grit. Further details are provided in Ref 17.

Coated and comparative uncoated fatigue test specimens were shot peened at Metal Improvement Company according to AMS 2432 using conditioned cut stainless steel wire (CCW14) at an intensity of 16 N and coverage of 200%. Here, 100% coverage indicates 100% of the elapsed time of shot peening required for the entire surface area to have been impacted. Correspondingly, 200% coverage indicates 200% of this required time of shot peening was applied (Ref 18). After shot peening, all shot-peened specimens were heat-treated at 760 °C for 8 h, in a low partial pressure of oxygen ($\sim 1.4 \times 10^{-16}$ MPa) to promote interdiffusion between the coating and substrate for the coated specimens. The low partial pressure of oxygen was intended to help form a protective Cr_2O_3 chromium oxide layer on the surface.

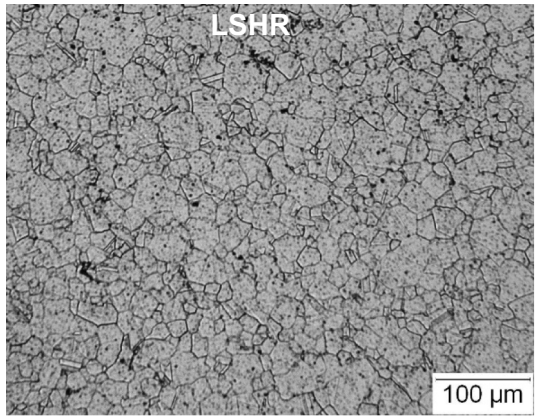

Fig. 1 Test material microstructures: (a) LSHR superalloy after solution and aging heat treatments, etched in waterless Kalling's reagent to show an average grain size of 15 μm, (b) NiCrY coating showing γ and α phases, after shot peening and interdiffusion heat treatment at 760 °C for 8 h

Table 1 Compositions of powder metal superalloy LSHR, cast & wrought alloy Nichrome, and cast alloys UCX and 50-50Nb in weight percent

Alloy – wt.%	Al	B	C	Co	Cr	Fe	Mn	Mo	Ni	Nb	O	Si	S	Ta	Ti	V	W	Y	Zr
LSHR	3.54	0.027	0.045	20.40	12.30	0.07	0.00	2.71	Bal.	1.49	0.02	0.012	< .0010	1.52	3.45	0.0055	4.28	< .0005	0.05
Nichrome	0.08				19.63	0.30	0.10		Bal.			1.315							
UCX			0.310		41.90	6.2	0.61	0.01	Bal.	0.01		2.000	0.002		0.20		0.72		
50-50Nb			0.014		48.28	0.001	0.00		Bal.	1.62		0.390	0.001						

The microstructure of the coating after these preparation steps is shown in Fig. 1(b). The coating had a mean thickness of 26.5 μm with a 95% confidence interval of $\pm$ 1.3 μm, using measurements of sections from unexposed test specimens. It consisted of a γ nickel-rich matrix with about 15 area percent of α chromium-rich precipitates.

Fatigue cycling was conducted in accordance with ASTM E466-96 in air on all test specimens, using a servo-hydraulic test machine with a resistance heating furnace that enclosed the specimen and specimen grips. Stress was cycled between maximum and minimum stress values of 841 and $-$ 427 MPa using a saw-tooth waveform at a frequency of 0.33 Hz. These stresses matched the stabilized maximum and minimum stresses produced by tests run on LSHR with strain cycled at a strain range of 0.76% and strain ratio (minimum/maximum strain) of 0 at 760 °C. LSHR which had been prepared, coated, shot peened and heat-treated as described here had a mean fatigue life of about 70,000 cycles at 760 °C. Uncoated specimens that were only machined, shot peened, and subjected to the same heat treatment as used for coated specimens also had a mean fatigue life of about 70,000 cycles at this temperature. However, individual specimen tests were interrupted here at 14, 700 and 35,000 cycles. These cycle intervals represent 0.02, 1, and 50% of the average coated fatigue life of 70,000 cycles that had been measured at 760 °C. Different specimens were interrupted at these different intervals of fatigue cycles at 760 °C and at room temperature. The average fatigue life of coated test specimens using the same applied stresses at room temperature was estimated to be about 100,000 cycles.

Selected coated and uncoated fatigue test specimens were examined before and after fatigue testing. Residual stresses were measured at the gage surface using a Bruker D8 Discover (area detector) x-ray diffractometer aligned in accordance with the approach and error bounds specified in ASTM E 915-10, but applied to the side-inclination rather than iso-inclination method. Further details are provided in Ref 17. These x-ray results were analyzed using the Bruker LEPTOS v.7 software. Average roughness was measured using a Zygo NewView 7200 white light interferometer, with a 10 $\times$ objective lens magnification having a resolution of 0.001 μm. Gage surfaces were also examined using a JEOL 6100 scanning electron microscope (SEM) at magnifications up to 5000$\times$.

Locations near one end of the gage surface were also electro-polished to various depths, in order to measure the variation in residual stresses with depth from the surface (Ref 17). The effect of removing material on the subsequently measured stresses was determined using the appropriate stress relationships (Ref 19), so that stresses could be corrected to account for this layer removal. Transverse sections were then sliced from the gage of each fatigue specimen and metallographically prepared for examination in the SEM.

The remaining gage sections of selected specimens were then subjected to an accelerated hot corrosion test. These specimen sections were corroded in air, by first coating them with a salt

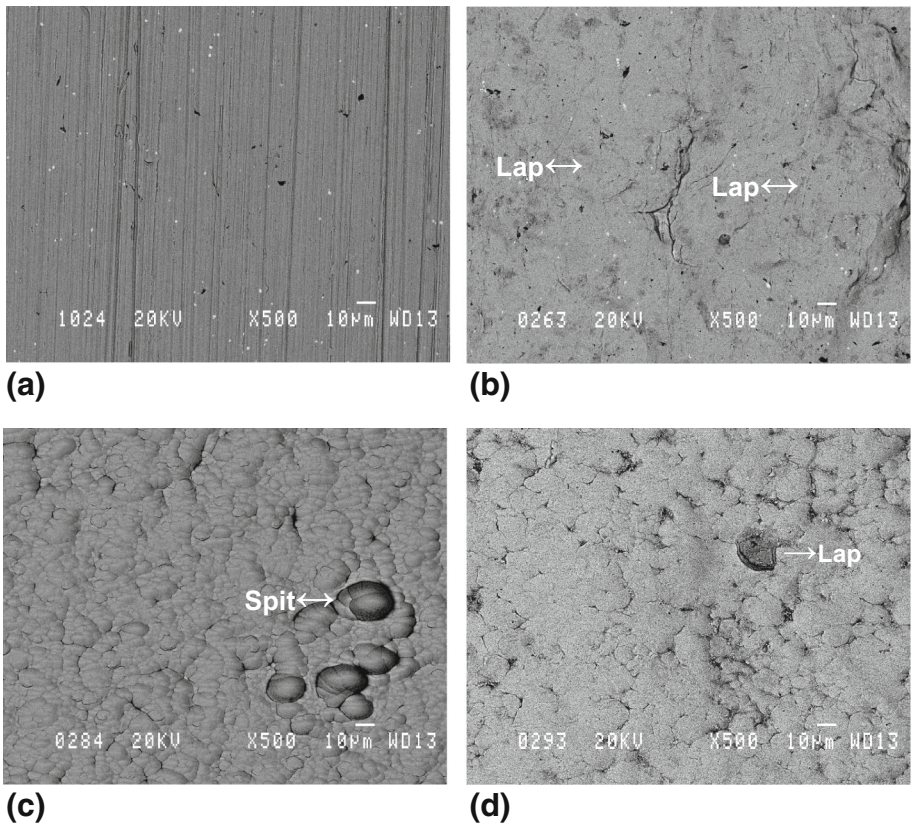

Fig. 2 Effects of specimen preparation steps on surface appearance: (a) uncoated specimen after machining, (b) uncoated specimen after machining, shot peening, and interdiffusion heat treatment, (c) coated specimen after coating application with "spits" from the coating process, (d) coated specimen after subsequent shot peening and interdiffusion heat treatment. "Laps" from the shot peening process are indicated. The fatigue loading direction is oriented vertically

mixture of 59 wt.% Na_2SO_4 and 41 wt.% $MgSO_4$ applied at 2 mg/cm^2 (Ref 17). Prior work indicated that uncoated LSHR test specimen sections salt coated in this manner and tested at 760 °C in air nucleated and grew corrosion pits within just 24 h. The resulting pits had a substantial effect on fatigue lives (Ref 20). Coated and uncoated fatigue specimen sections which were given this corrosion for 50 h were again examined in the SEM for the presence of pits.

Thermal expansion tests of LSHR and the coating alloys were performed with a Netzsch DIL 402 C push-rod dilatometer following ASTM E228-11, using sapphire as the standard. The tests were performed in an environment of argon flowing at 40 mL/min. Specimens were heated at a rate of 2 °C/min up to 815 °C, held at 815 °C for 10 min, and then cooled at − 2 °C/min to near room temperature. One specimen for each alloy was subjected to a single heating/cooling cycle. A second specimen was subjected to three of these thermal cycles, with 10-min isothermal segments at both ends, in order to measure repeatability and if the thermal strains changed with cycling.

Tensile tests of LSHR and the coating alloys were performed in general accordance with ASTM E8-16a and ASTM E21-09 in air, using a servo-hydraulic test machine with a resistance heating furnace integrated to enclose the specimen and specimen grips, and an axial extensometer attached to the specimen gage to maintain a strain rate of 0.5%/min. However, these tests were interrupted at a total strain of 1% and subsequently held at this strain for 24 h to measure the relaxation of stress. The coating alloy specimens were then cooled to room temperature, and a tensile test again run with an axial extensometer to maintain a strain rate of 0.5%/min. These tests were interrupted at a total strain of 1%, the extensometer was removed, and the tensile tests were continued to failure with displacement controlled to produce a rate of 0.104 mm/min. This displacement rate gave an average estimated strain rate across the effective gage length of 0.5%/min.

3. Results and Discussion

Typical SEM images of the surfaces are compared in Fig. 2 after (a) initial machining, (b) machined plus shot peened plus heat-treated, (c) initial coating, and (d) coated plus shot peened plus heat-treated. Machined specimens had very fine polishing grooves in the axial direction. Grit blasting and coating this surface eliminated the axial-grooved texture. The coating had scattered "spits" or coating nodules (Fig. 2), observed for all coated test specimens. These are believed to form from random arcing events in the plasma. So the coating had a rougher appearance over that of the machined surface. The shot-peened and heat-treated surfaces were more uniform, with the formerly grooved and nodular surface textures mostly eliminated, being replaced with an undulating, dimpled texture. Shot peening of the uncoated and coated surfaces resulted in folds of metal ("laps"), created by the impacts of shot (Fig. 2).

Measured average surface roughness and peak-to-valley roughness are compared in Fig. 3. Although more uniform in texture, shot peening increased the corresponding roughness of uncoated specimens, and both roughness parameters became more similar for uncoated and coated specimens that were shot peened and heat-treated, Fig. 3. Here, uncoated specimens had slightly higher roughness values than measured for coated specimens.

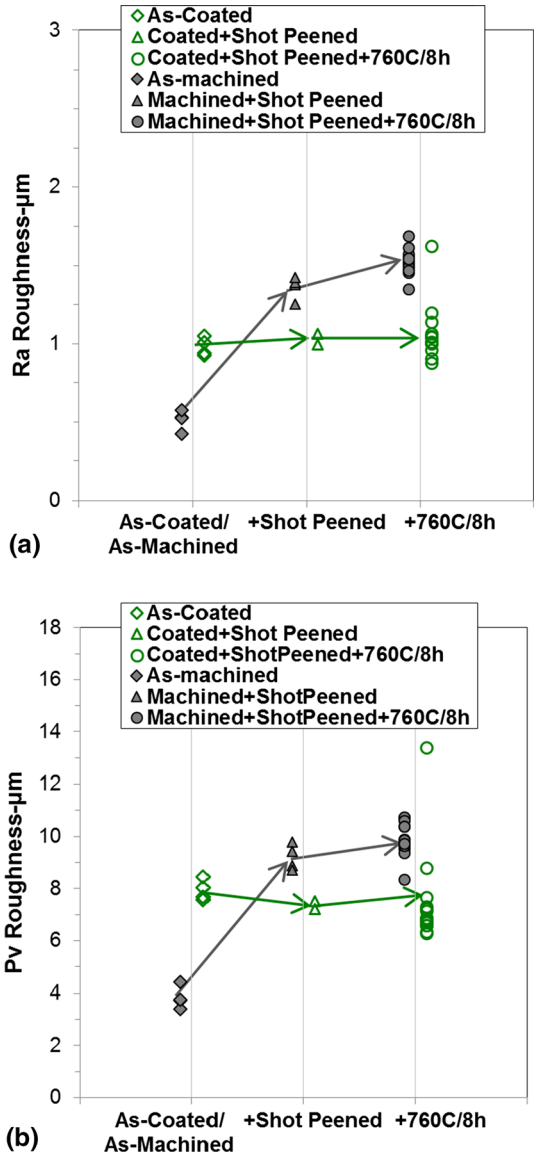

Fig. 3 Effects of specimen preparation steps on surface roughness: (a) average roughness (Ra) and (b) peak-to-valley roughness (Pv). Shot peening increased the roughness values of uncoated specimens (filled symbols), while roughness was maintained in coated specimens (hollow symbols)

The residual stresses measured at the surface before fatigue cycling are compared in Fig. 4. Machining of the fatigue test specimens produced a compressive axial residual stress of approximately − 200 MPa at the surface. However, coating of this surface changed the residual stress, producing tensile surface residual stresses around 200 MPa in the coating. It is recognized that various coating processes can themselves introduce varied residual stresses in coatings of similar composition. Yet, this was curious as the present coating process utilized physical vapor deposition, which did not have the high-speed impacts of solid particles such as in cold spraying of coatings (Ref 21). Subsequent shot peening produced comparable compressive residual stresses for both uncoated and coated surfaces. The final heat treatment at 760 °C for 8 h relaxed compressive surface residual stresses for

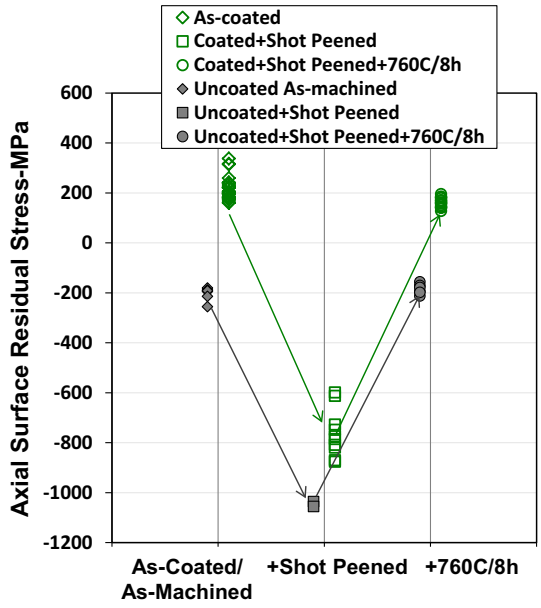

Fig. 4 Effects of specimen preparation steps on the surface residual stresses in the axial loading direction. Shot peening produced closer compressive residual stresses for uncoated (filled symbols) and coated (hollow symbols) surfaces. Heat treatment at 760 °C for 8 h relaxed out much of these compressive residual stresses at the surface

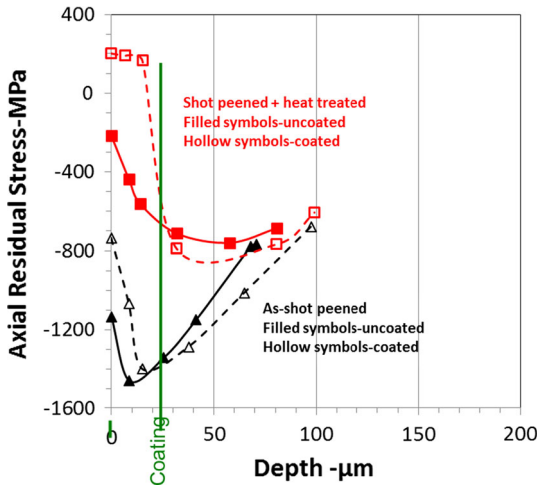

Fig. 5 Comparison of axial residual stresses near the surface for uncoated (filled symbols) and coated (hollow symbols) test specimens that have been shot peened, before (black symbols) and after (red symbols) the interdiffusion heat treatment. Shot peening produced greater compressive axial residual stresses for uncoated and coated test specimens within the near-surface region of 100 μm. Substantial compressive residual stresses remained in the substrate after heat treatment, but the entire coating came into tension

both uncoated and coated surfaces. Hence, the fully prepared uncoated specimens had a modest compressive residual stress measured at the surface of approximately − 200 MPa. Fully prepared coated specimens again had a modest tensile residual stress of near + 200 MPa. The generation of compressive residual stresses in the coating by shot peening has been described for MCrAlY coatings applied by various processes (Ref 22) and for NiCr coatings on superalloys (Ref 23). However, the complete relaxation of these compressive stresses in the coating during subsequent exposures to 760 °C was not expected. The reasons for this response of the coating will be considered in a later section. Very similar trends were also present for residual stresses measured transverse to the axial loading direction (Ref 17).

These surface measurements suggested beneficial compressive residual stresses from shot peening were largely eliminated by heat treatment. Yet, for both coated (filled symbols) and uncoated (hollow symbols) test specimens, axial residual stresses also varied significantly with depth, when comparing shot-peened test specimens before and after heat treatment, Fig. 5. Shot peening (black symbols) produced beneficial compressive residual stresses for both uncoated and coated test specimens within the near-surface region of 100 μm depth, which were greater in magnitude than those measured at the surface. The magnitudes of compressive axial stresses at and adjacent to the surface were reduced by the subsequent heat treatment (red symbols), especially within 25 μm of the surface for the coated specimens. At depths of over 25 μm, these reductions were more modest and comparable for coated and uncoated specimens. Overall, substantial compressive residual stresses of at least −500 MPa remained for both coated and uncoated specimens at depths of about 25 μm to over 100 μm. Therefore, in these regions, shot peening still did have lasting beneficial effects on residual stresses after heating, even in coated specimens. Similar partial relaxation of compressive residual stresses from shot peening by exposures at high temperatures has also been reported for similar though uncoated powder metal disk superalloys such as IN100 (Ref 24) and Rene 95 (Ref 15). Comparable results were again observed for residual stresses versus measured transverse to the axial loading direction (Ref 17).

Test specimens were then subjected to fatigue cycling that was interrupted at 14, 700 and 35,000 cycles. These cycle intervals represent 0.02, 1, and 50% of the average fatigue life of 70,000 cycles that had been measured at 760 °C. Typical surface appearance after fatigue cycling is compared in Fig. 6. No fatigue cracks were observed for most combinations of fatigue test temperature and cycle intervals. The surface roughness was stable with continued fatigue cycling, with uncoated values remaining slightly higher than those for coated test specimens, Fig. 7. However, fatigue cycling of a coated test specimen at 760 °C to 35,000 cycles produced scattered cracks which were relatively flat and normal to the axial loading direction (Fig. 6). These cracks ranged from 23 μm to 580 μm wide and had an average number density of 5.5 cracks/mm^2. Coating crack formation during fatigue cycling at certain conditions for NiCoCrAlY coatings on superalloy substrates has often been reported for turbine blade superalloys, usually attributed to the low ductility of their β NiAl phase at temperatures below about 870 °C (Ref 12). Yet, the fatigue cracking in the present study of such a presumed ductile NiCrY coating was not expected.

The residual stresses measured at the surface were stable with continued fatigue cycling in most cases. Residual stresses (Fig. 8) were stable for coated test specimens (hollow symbols) at both test temperatures, even when the scattered axial cracks were observed at 760 °C after cycling for 35,000 cycles. However, the axial residual stresses became more compressive for uncoated specimens (filled symbols) with continued cycling at 760 °C. This change in axial residual

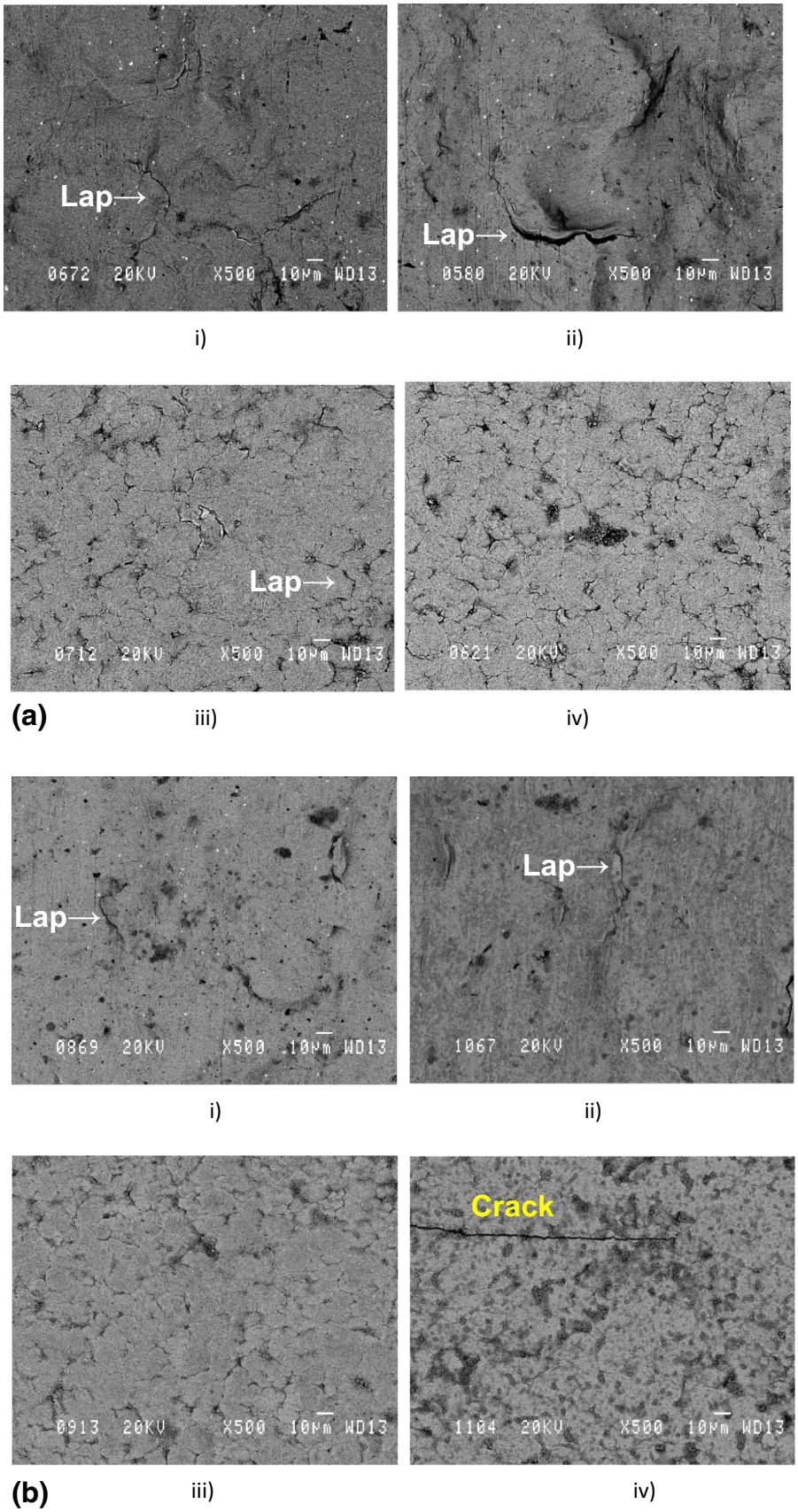

Fig. 6 (a) Comparison of typical surface appearance after interrupted fatigue cycling at 25 °C: (i) uncoated, 700 cycles, (ii) uncoated, 35,000 cycles, (iii) coated, 700 cycles, (iv) coated, 35,000 cycles. The fatigue loading direction is oriented vertically. (b) Comparison of typical surface appearance after interrupted fatigue cycling at 760 °C: (i) uncoated, 700 cycles, (ii) uncoated, 35,000 cycles, (iii) coated, 700 cycles, (iv) coated, 35,000 cycles. The fatigue loading direction is oriented vertically

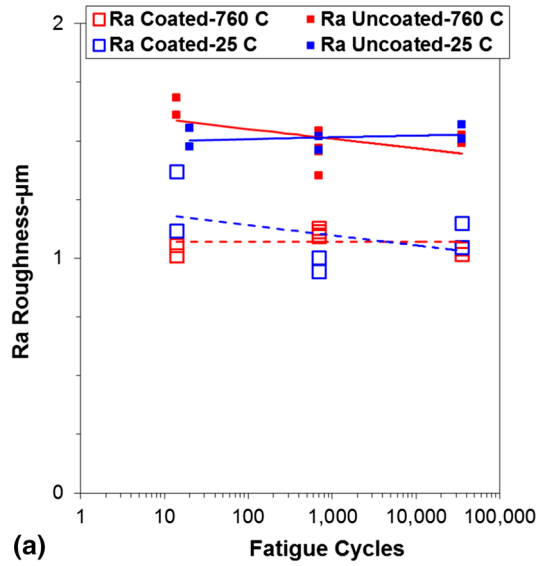

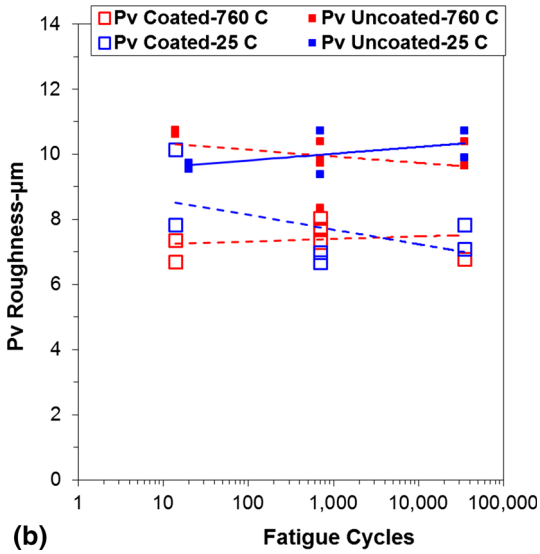

Fig. 7 Surface roughness parameters: (a) Ra and (b) Pv after interrupted fatigue cycling. The surface roughness was fairly stable with continued fatigue cycling, and uncoated (hollow symbols) values remained slightly higher than for coated (filled symbols)

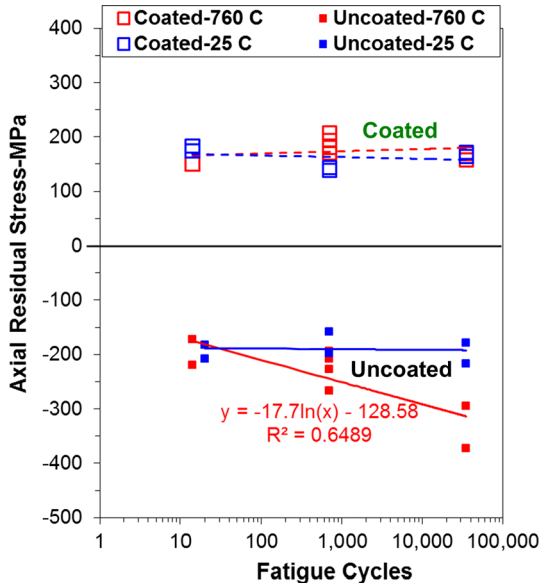

Fig. 8 Surface residual stresses in the axial loading direction, after interrupted fatigue cycling. The surface residual stresses were stable with continued fatigue cycling in most cases, but axial stresses for uncoated specimens (filled symbols) became more compressive at 760 °C (red symbols) with increasing cycles

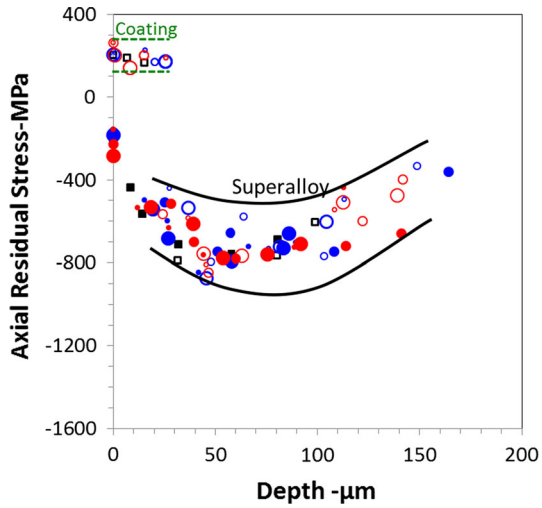

Fig. 9 Axial residual stress vs. depth near the surface after interrupted fatigue cycling of uncoated (filled symbols) and NiCrY-coated (hollow symbols) specimens. Residual stresses were stable (within the lined bands) with fatigue cycling in the coating and in the superalloy. Larger symbols indicate more fatigue cycles before interruption

stresses appeared to be driven by the fatigue cycling, as the applied loads were in this axial direction. This may be associated with cyclic hardening. The trend was apparent after just 700 fatigue cycles, which required only 35 min. Since the 8-h heat treatment resulted in a significant decrease in the compressive stress (Fig. 4), this increase in compressive stress indicates that the change in residual stress is due to fatigue cycling at 760 °C and not associated with the short time at this temperature. The trend was not apparent on the surface of the coated specimens.

The residual stresses as a function of depth were also surprisingly stable with continued fatigue cycling in this region, Fig. 9. Axial residual stress as a function of depth was stable for coated (filled symbols) and uncoated (hollow symbols) test specimens at both test temperatures. Increased intervals of fatigue cycles are indicated by increased symbol size, and the stress levels remained within a common band (dashed line). This was so even when the scattered axial coating cracks were observed at 760 °C after cycling for 35,000 cycles. Other studies have reported greater reductions in compressive residual stresses with initial fatigue cycles of finer grain disk superalloys IN100 (Ref 24) and Udimet 720Li (Ref 25), which then were stable during continuous cycling. The extent of these initial reductions have been shown to depend on the specific material's mechanical properties, the plasticity resulting from

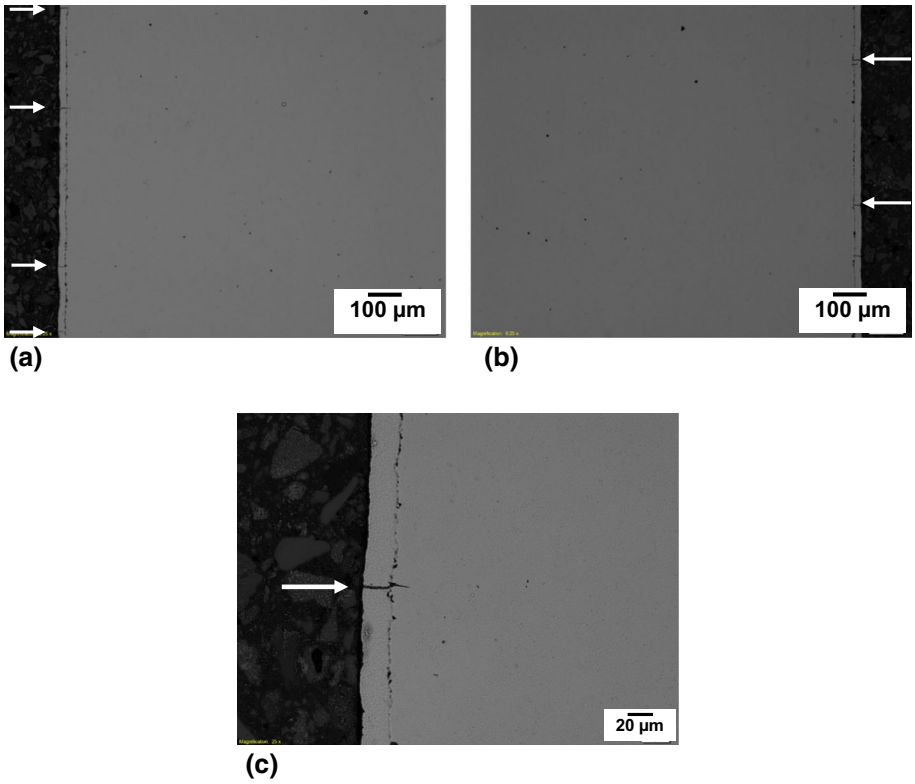

Fig. 10 Images from the longitudinal section prepared from a coated fatigue specimen after 35,000 fatigue cycles at 760 °C. The axial fatigue loads were applied in the vertical direction. Scattered cracks (arrows) occurred in the coating along the specimen surface. A majority of the fatigue cracks did not penetrate into the underlying superalloy. (a), (b) Typical distribution of cracks at mid-gage length; (c) deepest crack observed

prior shot peening conditions, the specific fatigue cycles, and the specific test temperature (Ref 26). For example, fatigue cycles inducing larger plastic strains have been shown to induce greater initial reductions in these compressive residual stresses (Ref 25). Significant compressive residual stresses remained below the surface for both coated and uncoated test specimens in the present test conditions, indicating that the coating did not significantly change the static and cyclic stress relaxation response in the superalloy.

Images from a metallographic section prepared parallel to the loading direction after 35,000 fatigue cycles at 760 °C are shown in Fig. 10, to further examine the condition of the coating at this point. Scattered fatigue cracks occurred in the coating along the specimen surface. However, a majority of the cracks did not penetrate into the underlying superalloy. The sectioned cracks that did continue to grow into the superalloy extended in by less than 15 μm. This was consistent with the remaining compressive residual stresses measured in the superalloy substrate, which could retard the growth of fatigue cracks.

Images of coated and uncoated test specimen surfaces subjected to 50 h of hot corrosion with subsequent ultrasonic cleaning in water to remove any remaining salt and soluble reaction product are shown in Fig. 11. Shot-peened plus heat-treated test specimen surfaces are compared to those also given 35,000 fatigue cycles at room temperature or 760 °C, each then corroded 50 h. The exterior surfaces of coated and uncoated test specimens were covered in Cr_2O_3 oxide, initially formed during heat treatment. Yet, scattered large pits exposing the substrate beneath the surface oxide were also evident in the uncoated test specimens. For the coated test specimens, the oxide was attacked in places, but no open corrosion pits exposing the substrate were observed, even for specimens fatigue tested to 700 cycles or 35,000 cycles before hot corrosion. A higher magnification backscatter electron image (BSE) of typical sectioned samples subjected to 35,000 cycles at 760 °C and 50 h of hot corrosion showed the coating was largely intact, Fig. 12. Hence, for at least up to 50% of the expected LCF lifetime at 760 °C and in the presence of cracks, the coating continued to protect the superalloy substrate from corrosion attack for the conditions evaluated. It appears that even after 35,000 fatigue cycles at 760 °C, the scattered fatigue cracks did not provide open sites for pits to form in the underlying superalloy. Prior work showed that without shot peening of the coating, a similar Ni-35Cr-0.1Y (weight percent) coating still protected this superalloy from corrosion pitting after up to 1000 h of thermal cycling between 25 and 760 °C (Ref 16). Cold-sprayed coatings of very similar composition (Ni-50Cr in weight percent) with remnant porosity have also been shown to protect steel substrates from corrosion pitting (Ref 27). Hence, these NiCr coatings can continue to protect substrates from this corrosion in spite of some levels of flaws, including the porosity, oxidation, or fatigue cracking observed for these cases.

In further support of this point, a polished cross section with the present coating on a separate fatigue test specimen prepared with the same shot peening and heat treatment is shown for comparison in Fig. 13. This coated specimen had been subjected to oxidation exposure in air for 500 h at 760 °C and the hot corrosion test as above, followed by fatigue cycling

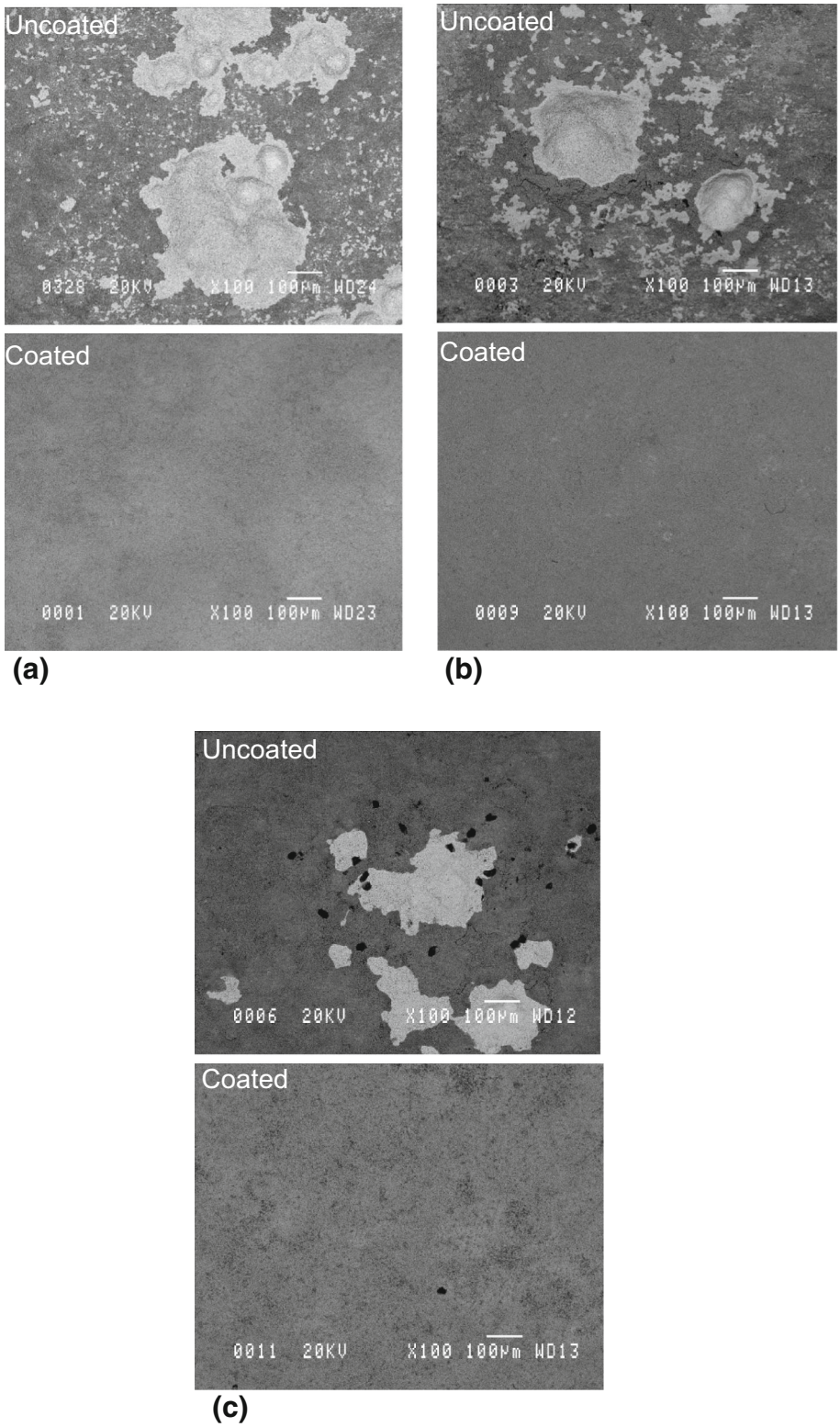

Fig. 11 Comparisons of typical surface appearance of uncoated and coated test specimens after hot corrosion at 760 °C for 50 h: (a) no fatigue cycles, (b) 35,000 fatigue cycles at room temperature, (c) 35,000 fatigue cycles at 760 °C. The coating prevented corrosion from exposing the substrate after even 35,000 fatigue cycles, with no open pits observed. The axial fatigue loading direction is horizontal

to failure at 760 °C, using the same applied stresses as before. Cracks can be seen penetrating the coating, but again show minimal extension into the substrate. Only the outer portion of the sample still contains the high-Cr alpha phase. Interdiffusion with the substrate, likely during the 500 h oxidation exposure, has resulted in recession of the alpha phase. Multiple secondary

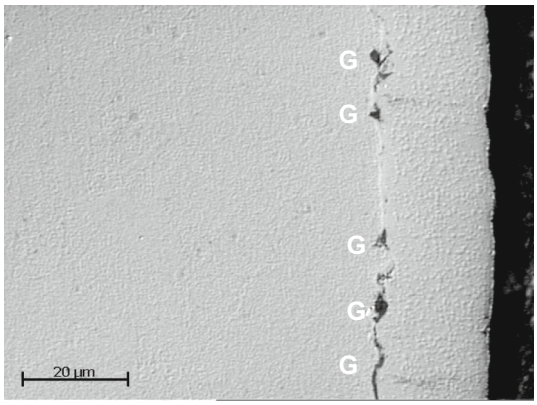

Fig. 12 Longitudinal section prepared from a coated fatigue specimen after 35,000 fatigue cycles at 760 °C, plus 50 h of hot corrosion at 760 °C. G-alumina grit particles embedded during grit blasting, before the coating process. The coating did not show pits extending into the underlying superalloy. The axial fatigue loads had been applied in the vertical direction

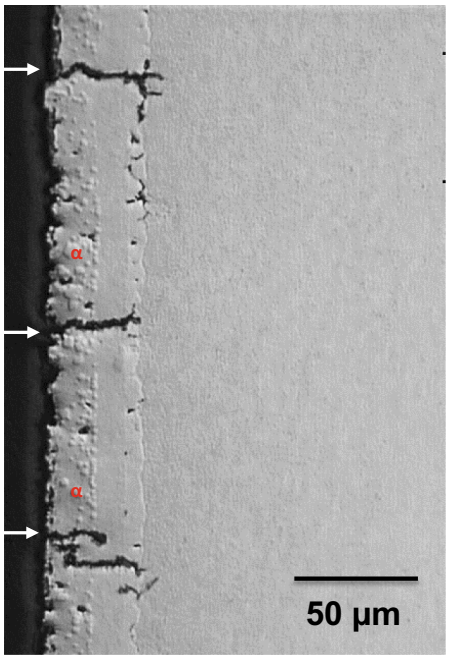

Fig. 13 Secondary cracks observed in longitudinal section prepared from a coated fatigue specimen that was subjected to 500 h of oxidation at 760 °C plus 50 h of hot corrosion at 760 °C, and then fatigue tested at 760 °C to failure. Multiple secondary fatigue cracks grew through the coating, but many still did not extend into the underlying superalloy. The axial fatigue load was applied in the vertical direction

fatigue cracks grew through the coating, but many still did not extend into the underlying superalloy. Again, no corrosion pits were found that penetrated completely through the coating during the corrosion treatment. Therefore, the coating did appear to be robust, in still protecting the substrate superalloy from corrosion attack and pit formation for the present test

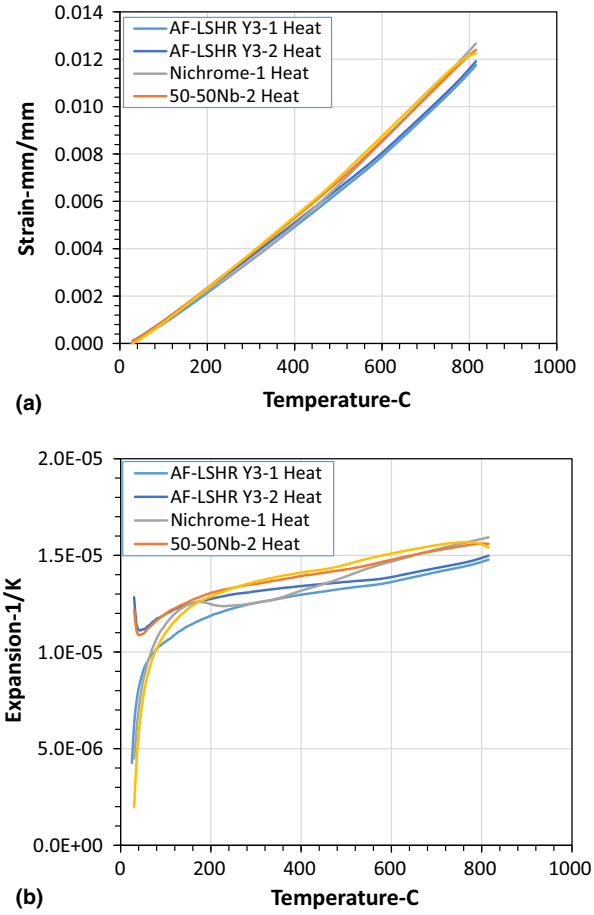

Fig. 14 Comparisons of: (a) typical thermal expansion strains, (b) mean coefficient of thermal expansion vs. temperature in LSHR and the coating alloys

conditions in the presence of these changes from extended oxidation exposures.

The persistence of tensile residual stresses in the coating, as measured at room temperature by x-ray diffraction, merited further consideration. It was notable that these tensile stresses were first measured in the coating after coating application. While shot peening did succeed in shifting these stresses to be compressive and of higher magnitudes, subsequent heat treatment at 760 °C restored the tensile residual stresses at room temperature to values near those originally measured. Therefore, it appeared the stresses could be related to excursions to high temperatures.

Hence, specimens of LSHR and of "coating alloys" having compositions near that of the coating were prepared of consistent size and tested for linear coefficient of thermal expansion (CTE) up to 815 °C. The resulting time–temperature expansion strain responses are compared in Fig. 14(a). The LSHR substrate alloy displayed lower thermal expansion strains than all the coating alloys. The corresponding mean linear coefficient of thermal expansion is shown versus temperature in Fig. 14(b), showing the same trend for this calculated value. Second specimens of each alloy were subjected to three repeated thermal cycles in order to confirm this response and to allow estimates of variability in the

response. LSHR, cast UCX, and cast 50-50Nb had very consistent response. However, the repeated cycles of Nichrome produced higher CTE values than for the initial cycle, as shown in Fig. 15. This could be related to remnant deformation from the cold drawing process used to produce the Nichrome bar, which was annealed out during the first cycle. The resulting stabilized mean linear coefficients of thermal expansion with 95% confidence intervals are indicated in Fig. 16, affirming that the coating alloys did have significantly higher thermal expansion than LSHR. These values are tabulated in Table 2.

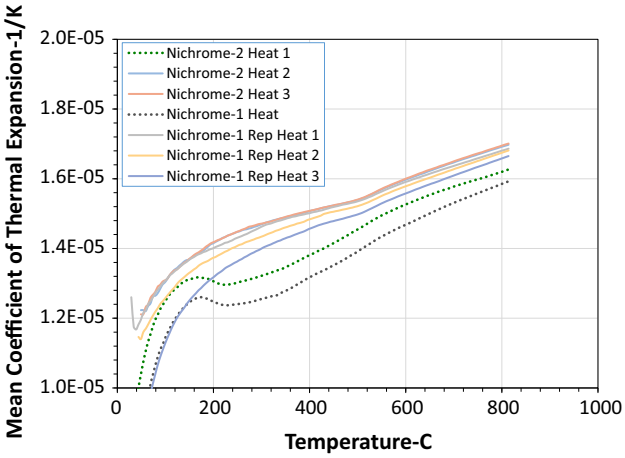

Fig. 15 Comparison of the mean coefficient of thermal expansion vs. temperature for Nichrome specimens over repeated cycles. The initial cycle gave lower expansion than subsequent cycles for each Nichrome specimen

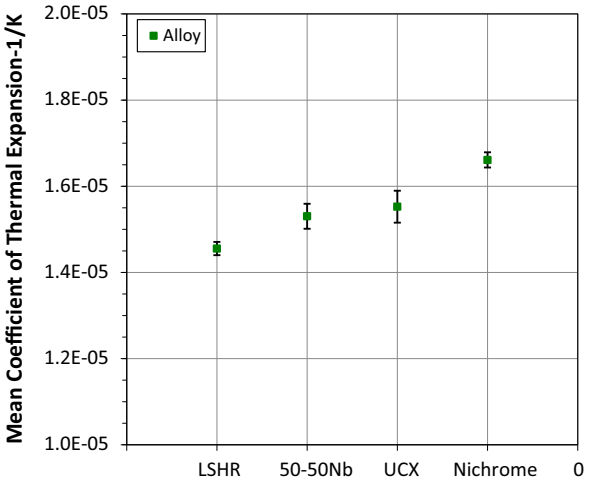

Fig. 16 Comparisons of mean coefficient of thermal expansion to 760 °C for LSHR and the coating alloys. The bars indicate a 95% confidence interval for each value, over 4-5 cycles

The residual stresses that can be generated due to differences in thermal expansion between coatings and substrates have been considered in various levels of complexity ranging from uniaxial analytical elastic models that consider only thermal mismatch strains to finite element modeling that consider thermal mismatch strains as well as transient effects of the coating application process, for example (Ref 27-31). A simple analytical approach considering only elastic strains generated by thermal mismatch was used for an initial evaluation, using available data and these materials. When the coating/substrate pair has a coating thickness much smaller than the substrate radius, the axial and transverse elastic residual stresses ($\sigma_a \approx \sigma_t$) in the coating have been estimated (Ref 27-30) as:

$$\sigma_a \approx \sigma_t = E_c/(1-\nu_c)(\alpha_c - \alpha_s)\left(T_{eq} - T\right), \qquad \text{(Eq 1)}$$

where E_c is Young's elastic modulus of the coating, ν_c is Poisson's ratio of the coating, T_{eq} is the temperature at which the coating and substrate are at equilibrium and stress free, and T is the temperature at which the stresses are evaluated. Experimental verifications of residual stresses using digital image correlation (Ref 29) and using x-ray diffraction (Ref 30) have indicated that this is a reasonable first approximation. For the present study, the substrate and coating were estimated to be at a temperature near 760 °C upon deposition, and so the substrate and coating were assumed to be stress free at that temperature. Table 2 includes typical values from the suppliers for Young's elastic modulus and Poisson's ratio, along with the calculated residual stresses in the coating. The calculated residual stresses in the coating alloys at room temperature are near that measured in the coated fatigue specimens by x-ray diffraction.

One important aspect in considering this estimation of stresses generated in the coating is the stress-bearing capability of the coating alloys. The coating is not strengthened by gamma prime precipitates as is the LSHR and should be weaker than this substrate. Tensile tests were therefore performed at 760 °C, an approximate maximum temperature of the coating/substrate in some applications, and also the temperature used in the heat treatment for 8 h of the coated fatigue specimens after shot peening. However, these tensile tests were interrupted and held at a strain of 1% for 24 h to assess how much relaxation of any

Table 2 Thermal expansion and tensile stress relaxation responses for LSHR and "coating alloys" near the coating composition

Alloy	Young's Modulus at 25 °C-GPa	Poisson's Ratio	Measured Mean Coef. Of Thermal Expansion 25 °C to 760 °C-μstrain/°C	Estimated Thermal Contraction Stress in the Coating at 25 °C (Eq 1)-MPa	Yield Strength at 760 °C-MPa	Relaxed Stress at 760 °C/1%/8 h-MPa
LSHR	226	0.286	14.56		993	524
Nichrome	213	0.29	16.61	451	316	88
UCX	207	0.29	15.53	208	214	33
50-50Nb	176	0.29	15.3	135	169	30

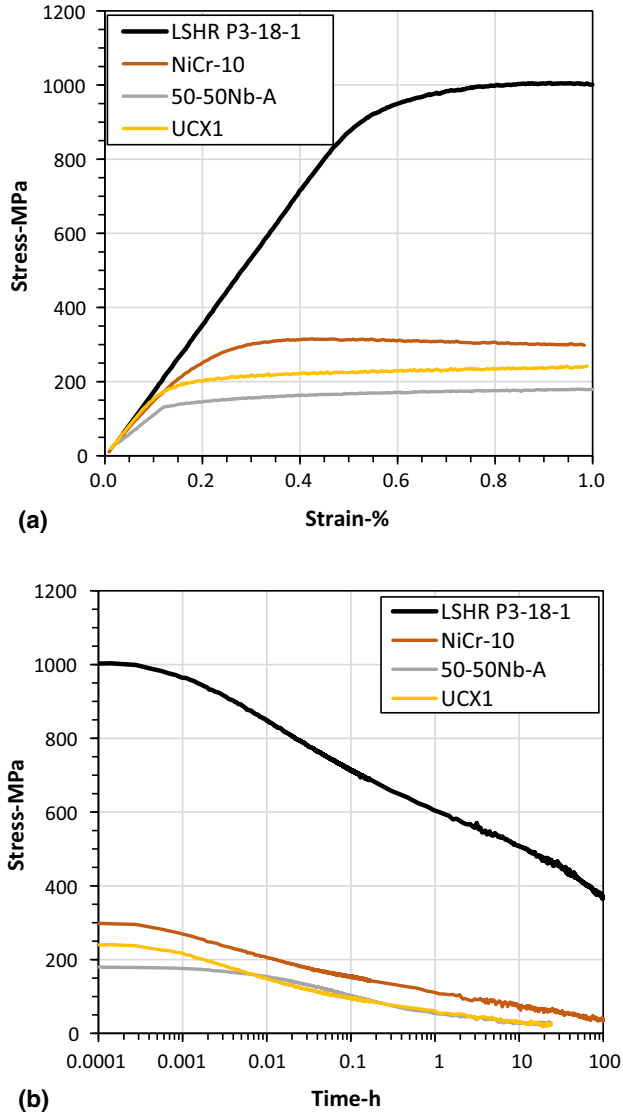

Fig. 17 Comparisons of typical LSHR and coating alloy responses at 760 °C to: (a) tensile tests interrupted at 1% strain, (b) subsequent stress relaxation at 1% strain

generated stresses can occur in the alloys at this temperature, as shown in Fig. 17. Among the coating alloys, the lowest average yield strength ranged from 169 MPa observed for 50-50Nb to 316 MPa measured for Nichrome. LSHR had much higher average yield strength of 993 MPa. During subsequent stress relaxation at 1% strain (Fig. 17b), the coating alloys all relaxed stresses far more rapidly and to greater magnitudes than for LSHR. Among the coating alloys, stresses sustained after 8 h relaxation ranged from only 30 MPa for 50-50Nb to 88 MPa for Nichrome, Table 2. These values for the coating alloys were far lower than the stress of 524 MPa sustained by LSHR after 8 h of relaxation. The finer grain size of the actual applied coating could give higher yield strength, but lower resistance to stress relaxation than measured for the coarse grain coating alloys tested here. So these tensile stress relaxation tests were judged still useful for initial engineering estimates of the resistance of the coating to stress relaxation, in comparison with that of LSHR. Clearly, the coating could support very little residual stress at 760 °C. But the coating could support residual stresses when subsequently cooled down to room temperature, where yield strengths exceeding 300 MPa are reported (Ref 32).

Therefore, the modest tensile residual stresses measured by x-ray diffraction after coating the specimens and cooling to room temperature were consistent with the higher coefficients of thermal expansion measured in the coating alloys than in the substrate superalloy LSHR. While subsequent shot peening did generate compressive residual stresses in the coating, at temperatures near 760 °C these stresses in the coating would quickly relax to near zero. Hence, tensile residual stresses would again be generated when cooling from this temperature, due to the higher thermal contraction of the coating than of the substrate superalloy. The lack of compressive residual stresses in the coating after shot peening plus heat treatment helped account for the earlier cracking of the coating during fatigue cycling. Yet, the substantial compressive residual stresses retained in the superalloy substrate impeded crack growth there, and held the coating cracks tightly closed. Hence, the coating could still protect the superalloy substrate from corrosion pitting.

4. Summary of Results

LSHR fatigue test specimens were coated with a NiCrY coating, and then shot peened and heat-treated along with uncoated test specimens. Shot peening made average roughness more uniform, but the induced compressive residual stresses relaxed at the surface during subsequent heat treatment for both coated and uncoated test specimens. Modest tensile residual stresses were generated in the coating, related to the greater thermal contraction of the coating than of the substrate. Yet, significant compressive residual stresses remained below the surface of the substrate for both the coated and uncoated cases. Following shot peening and heat treatment, both coated and uncoated specimens were fatigue cycled at room temperature and at 760 °C for up to half the average LCF lifetime previously measured at 760 °C. For both the coated and uncoated case, the surface roughness and residual stresses remained stable, except that the axial residual stress at the surface for the uncoated specimen became more compressive with continued cycling at 760 °C. In addition, for the coated sample, cracks appeared in the coating after the longest period of cycling (35,000 cycles) at 760 °C. Following the fatigue cycling, sections of each sample were corroded at 760 °C for 50 h. Corrosion pits were observed to form on the uncoated samples. However, although the thin surface oxide was attacked on the coated samples, no corrosion pits were observed even where fatigue cracks existed in the coating. Tests of alloys near the coating's composition indicated modestly higher thermal expansion, along with much lower strength and stress relaxation resistance of the coating than the superalloy substrate can explain the coating's stress response. The resulting residual stresses allowed enhanced cracking of the coating, but impeded growth of these cracks in the superalloy substrate.

5. Conclusions

This examination of the influences that processing and fatigue cycling have on residual stresses in a NiCrY-coated powder metallurgy disk superalloy showed:

1. Shot peening can make the roughness of coatings more uniform, but the induced compressive residual stresses at the surface relax in this coating at high temperatures.

(a) Differences in thermal expansion coefficient between the coating and superalloy substrate can then result in modest tensile residual stresses in the coating near room temperature.
(b) Yet, substantial compressive residual stresses can still remain below the surface in the substrate.

2. The shot-peened surface can remain intact during continued fatigue cycling with stable roughness and residual stresses for most cases, except for longest cycling at 760 °C:

(a) For uncoated test specimens, axial residual stresses can become more compressive with cycling and surface cracking is not expected until after 35,000 cycles.
(b) For coated specimens, cracks can begin to form sooner in the coating, consistent with the above elimination of compressive residual stresses in the coating. Yet, the adjacent substrate can retain stable compressive residual stresses, sufficient to continue suppressing fatigue crack growth into the substrate.

3. Corrosion resistance in air at 760 °C for 50 h is not strongly impacted by this fatigue cycling:

(a) For uncoated specimens, the oxide layers formed during such intervals of fatigue cycling at 760 °C are not sufficiently protective to prevent corrosion pits from still reaching the substrate.
(b) For coated specimens, the NiCrY coating can remain protective after these intervals of fatigue cycling to continue preventing these pits from forming, even when fatigue cracks have begun to form, or after extended oxidation.

Acknowledgments

The authors would like to acknowledge the hard work of Dr. Ronghua Wei/Southwest Research Institute for coating the specimens, Don Humphrey and John Setlock/Zin Technologies, Inc. for heat treating the specimens, Chantal Sudbrack/NASA GRC for imaging of some sections of coated specimens and reviewing this manuscript, and Sai Raj/NASA GRC for consultation on the thermal expansion results. Michael Gyorffy/Kubota Metal Corporation is gratefully acknowledged for supplying samples of cast alloys UCX and 50-50Nb.

References

1. R. Schafrik and R. Sprague, Superalloy Technology—A Perspective on Critical Innovations for Turbine Engines, *Key Eng. Mater.*, 2008, **380**, p 113–134
2. M.R. Bache, J.P. Jones, G.L. Drew, M.C. Hardy, and N. Fox, Environment and Time Dependent Effects on the Fatigue Response of an Advanced Nickel Based Superalloy, *Int. J. Fatigue*, 2009, **31**(11–12), p 1719–1723
3. A. Encinas-Oropesa, G. Drew, M. Hardy, A. Leggett, J. Nicholls, and N. Simms, *Effects of Oxidation and Hot Corrosion in a Nickel Disc Alloy, Superalloys 2008*, R. C. Reed, K. A. Green, P. Caron, T. P. Gabb, M. A. Fahrmann, E. S. Huron and S. A. Woodard, Ed., Sept 14–18, 2008 (Champion, PA), The Mining, Metallurgy, and Materials Society, 2008, p 609–618
4. C. K. Sudbrack, S. L. Draper, T. Gorman, J. Telesman, T. P. Gabb, and D. R. Hull, *Oxidation and the Effects of High Temperature Exposures on Notched Fatigue Life of an Advanced Powder Metallurgy Disk Superalloy, Superalloys 2012*, E. S. Huron, R. C. Reed, M. C. Hardy, M. J. Mills, R. E. Montero, P. D. Portella and J. Telesman, Ed., Sept 9–13, 2013 (Champion, PA), The Mining, Metallurgy, and Materials Society, 2012, p 863–872
5. R.A. Rapp, Hot Corrosion of Materials: A Fluxing Mechanism?, *Corros. Sci.*, 2002, **44**, p 209–221
6. F.S. Pettit and C.S. Giggins, *Hot Corrosion, Superalloys II*, C.T. Sims, N.S. Stoloff, and W.C. Hagel, Ed., Wiley, New York, 1987, p 327–358
7. B. Gleason, *High-Temperature Corrosion of Metallic Alloys and Coatings, Materials Science and Technology*, R.W. Cahn, P. Haasen, and E.J. Kramer, Ed., Wiley, New York, 2000, p 173–228
8. J. R. Groh, and R. W. Duvelius, *Influence of Corrosion Pitting on Alloy 718 Fatigue Capability, Superalloy 718, 625, 706 and Derivatives*, E. A. Loria, Ed., June 17–20, 2001(Pittsburgh, PA), The Mining, Metallurgy, and Materials Society, 2001, p 583–592
9. G.S. Mahobia, N. Paulose, S.L. Mannan, R.G. Sudhakar, K. Chattopadhyay, and N.C.S. Srinivas, Effects of Hot Corrosion on the Low Cycle Fatigue Behavior of IN718, *Int. J. Fatigue*, 2014, **59**, p 272–281
10. J.K. Sahu, R.K. Gupta, J. Swaminathan, N. Paulose, and S.L. Mannan, Influence of Hot Corrosion on the Low Cycle Fatigue Behavior of SU 263, *Int. J. Fatigue*, 2013, **51**, p 68–73
11. J. Telesman, T.P. Gabb, Y. Yamada, and S.L. Draper, Fatigue Resistance of a Hot Corrosion Exposed Disk Superalloy at Varied Test Temperatures, *Mater. High Temp.*, 2016, **33**(4–5), p 517–527
12. G.W. Goward, Progress in Coatings for Gas Turbine Airfoils, *Surf. Coat. Technol.*, 1998, **108–109**, p 73–79
13. G. Kappmeyer, C. Hubig, M. Hardy, M. Witty, and M. Busch, Modern Machining of Advanced Aerospace Alloys—Enabler for Quality and Performance, in *5th CIRP Conference on High Performance Cutting 2012*, K. Wegener, Ed., June 4–7, 2012, (Zurich, Switzerland), Elsevier B. V., 2012, p 28–43
14. P.S. Prevéy, X-Ray Diffraction Characterization of Residual Stresses Produced by Shot Peening, in *Shot Peening: Theory and Application*, J. Champaigne and J.S. Eckersley, Ed., IITT-International, Paris, 1991, p 81–93
15. M. K. Tufft, Shot Peen Impact on Life, Part 1: Development of a Fracture Mechanics/Threshold Behavior Predictive Model, Shot Peening Present & Future, in *Proceedings of the 7th International Conference on Shot Peening*, Sept 28-Oct 1, 1999 (Warsaw, Poland), Institute of Precision Mechanics, 1999, p 244–253
16. T. P. Gabb, R. A. Miller, C. K. Sudbrack, S. L. Draper, J. A. Nesbitt, R. B. Rogers, J. Telesman, V. Ngo, and J. Healy, *Cyclic Oxidation and Hot Corrosion of NiCrY-Coated Disk Superalloys*, NASA/TM-2016-219105, NASA, Washington, DC, June, 2016
17. T. P. Gabb, R. B. Rogers, J. A. Nesbitt, B. J. Puleo, R. A. Miller, J. Telesman, and S. L. Draper, *Residual Stresses in a NiCrY-Coated Powder Metallurgy Disk Superalloy*, NASA/TM-2017-219514, NASA, Washington, DC, June, 2017
18. J. T. Cammet, P. S. Prevéy, and N. Jayaraman, The Effect of Shot Peening Coverage on Residual Stress, Cold Work, and Fatigue in a Nickel-Base Superalloy, in *Proceedings of ICSP-9*, V. Schulze and A. Niku-Lari, Ed., Sept 6–9, 2005, (Paris, France), ISCSP, 2005, p 429–435
19. M.G. Moore and W.P. Evans, Mathematical Correction for Stress in Removed Layers in X-Ray Diffraction Residual Stress Analysis, *SAE Trans.*, 1958, **66**, p 340–344
20. J. Nesbitt and S.L. Draper, Pit Morphology and Depth After Low-temperature Hot Corrosion of a Disc Alloy, *Mater. Temp.*, 2016, **51**(4–5), p 501–516
21. N. Bala, H. Singh, and S. Prakash, X-ray Diffraction Study of Cold Sprayed Ni-20Cr and Ni-50Cr Coatings on Boiler, *Adv. Mater. Res.*, 2013, **620**, p 257–262
22. J. F. Loersch, and J. W. Neal, Peened Overlay Coatings, U. S. 4,514,469, U.S. Patent Office, Washington, DC, 1985
23. B. T. Hazel, and M. J. Weimer, Turbine Component Protected With Environmental Coating, U.S. 7,364,801 B1, U. S. Patent Office, Washington, DC, 2008

24. D. Buchanon, R. John, R. A. Brockman, and A. H. Rosenberger, *A Coupled Creep Plasticity Model for Residual Stress Relaxation of a Shot Peened Nickel-Base Superalloy*, R. C. Reed, K. A. Green, P. Caron, T. P. Gabb, M. A. Fahrmann, E. S. Huron and S. A. Woodard, Eds., Sept 14–18, 2008 (Champion, PA), The Mining, Metallurgy, and Materials Society, 2008, p 965–974
25. A. Evans, S.-B. Kim, J. Shackleton, G. Bruno, M. Preuss, and P.J. Withers, Relaxation of Residual Stress in Shot Peened Udimet 720Li Under High Temperature Isothermal Fatigue, *Int. J. Fatigue*, 2005, **27**, p 1530–1534
26. W.Z. Zhuang and G.R. Halford, Investigation of Residual Stress Relaxation Under Cyclic Load, *Int. J. Fatigue*, 2001, **23**(1), p 31–37
27. N. Bala, H. Singh, J. Karthikeyan, and S. Prakash, Cold Spray Coating Process for Corrosion Protection: A Review, *Surf. Eng.*, 2014, **30**(6), p 414–421
28. A.G. Evans, G.B. Crumley, and R.E. Demaray, On the Mechanical Behavior of Brittle Coatings and Layers, *Oxid. Met.*, 1983, **20**(5–6), p 193–216
29. R. J. Thompson and K. J. Hemker, Thermal Expansion Measurements on Coating Materials by Digital Image Correlation, in *Proceedings of the SEM Annual Conference and Exposition on Experimental and Applied Mechanics*, June 4–6, 2007 (Springfield, MA) 2007, p 1058–1067
30. A. J. McGinnis, T. R. Watkins, and K. Jagannadham, Residual Stresses in a Multilayer System of Coatings, in *Proceedings of the Denver X-ray Conference (DXC) on Applications of X-ray Analysis*, International Centre for Diffraction Data (ICDD), 1999, p 443–454
31. L. Wang, X.H. Zhong, Y.X. Zhuo, S.Y. Tsao, W. Zhang, Y. Wang, and X.G. Sun, Design and Optimization of Coating Structure for the Thermal Barrier Coatings Fabricated by Atomspheric Plasma Spraying via Finite Element Method, *J Asian Ceram Soc*, 2014, **2**, p 102–116
32. Heat and Corrosion Resistant Castings: Their Engineering Properties and Applications, Publication No. 266, Nickel Institute, p 1–52. https://www.nickelinstitute.org/en/TechnicalLibrary/INCO%20Series/0266_Heat_ResistantCastingsCorrosion_ResistantCastingstheirEngineeringPropertiesandApplications.aspx